J|A|C|S
ARTICLES
Published on Web 10/13/2006

Rotational Reorganization of Doped Cholesteric Liquid Crystalline Films

Rienk Eelkema,[†] Michael M. Pollard,[†] Nathalie Katsonis,[†] Javier Vicario,[†] Dirk J. Broer,[‡,§] and Ben L. Feringa*[,†]

Contribution from the Department of Organic and Molecular Inorganic Chemistry, Stratingh Institute, University of Groningen, Nijenborgh 4, 9747 AG Groningen, The Netherlands, Department of Polymer Technology, Faculty of Chemistry and Chemical Engineering, Eindhoven University of Technology, PO Box 513, 5600 MB Eindhoven, The Netherlands, and Philips Research Laboratories, Department of Biomolecular Engineering, High Tech Campus 4, 5656 AE Eindhoven, The Netherlands

Received July 25, 2006; E-mail: b.l.feringa@rug.nl

Abstract: In this paper an unprecedented rotational reorganization of cholesteric liquid crystalline films is described. This rotational reorganization results from the conversion of a chiral molecular motor dopant to an isomer with a different helical twisting power, leading to a change in the cholesteric pitch. The direction of this reorganization is correlated to the sign of the change in helical twisting power of the dopant. The rotational reorganization of the liquid crystalline film was used to rotate microscopic objects 4 orders of magnitude larger than the bistable dopants in the film, which shows that molecular motors and switches can perform work. The surface of the doped cholesteric liquid crystalline films was found to possess a regular surface relief, whose periodicity coincides with typical cholesteric polygonal line textures. These surface features originate from the cholesteric superstructure in the liquid crystalline film, which in turn is the result of the presence of the chiral dopant. As such, the presence of the dopant is expressed in these distinct surface structures. A possible mechanism at the origin of the rotational reorganization of liquid crystalline films and the cholesteric surface relief is discussed.

Introduction

Biological systems use molecular motors in almost every energy-dependent process they undertake, including cellular translocation, ion pumping, active molecular transport, and ATP synthesis.[1] In many of these capacities, the collective action of many biomolecular motors is harnessed to effect the movement of structures many times their size. The recent development of synthetic molecular systems including shuttles[2], rotors[3], muscles,[4] switches,[5] elevators,[6] motors[7−10] and processive catalysts[11] has brought the prospect of synthetic nanoscale "mechanical machines" within sight. As our understanding of how to design molecular motors has advanced, the central question surrounding them has shifted to how their action can be effectively applied to perform work. The application of molecular machines in the movement of larger-scale objects has, however, remained restricted to a few isolated cases, leaving most synthetic molecular-scale machines still to prove that they can do useful functions. Ichimura and co-workers first demonstrated the ability of azobenzene molecular switches to perform work by generating surface energy gradients, and used this system to translate liquid droplets.[12] This concept was subsequently applied by Picraux and co-workers using spiropyrans,[13] and Leigh, Zerbetto, Rudolf, and co-workers with rotaxanes.[14] Gaub successfully

[†] University of Groningen.
[‡] Eindhoven University of Technology.
[§] Philips Research Laboratories.

(1) (a) Stryer, L. Biochemistry, 4th ed.; W. H. Freeman: New York, 1995; Chapter 15. (b) *Molecular Motors*; Schliwa, M. Ed.; Wiley-VCH: Weinheim, 2003.
(2) (a) Pease, A. R.; Jeppesen, J. O.; Stoddart, J. F.; Luo, Y.; Collier, C. P.; Heath, J. R. *Acc. Chem. Res.* **2001**, *34*, 433−444. (b) Ballardini, R.; Balzani, V.; Credi, A.; Gandolfi, M. T.; Venturi, M. *Acc. Chem. Res.* **2001**, *34*, 445−455. (c) Keaveney, C. M.; Leigh, D. A. *Angew. Chem., Int. Ed.* **2004**, *43*, 1222−1224.
(3) (a) Dominguez, Z.; Khuong, T.-A. V.; Dang, H.; Sanrame, C. N.; Nunez, J. E.; Garcia-Garibay, M. A. *J. Am. Chem. Soc.* **2003**, *125*, 8827−8837. (b) Kuwatani, Y.; Yamamoto, G.; Iyoda, M. *Org. Lett.* **2003**, *5*, 3371−3374. (c) Hawthorne, M. F.; Zink, J. I.; Skelton, J. M.; Bayer, M. J.; Lui, C.; Livshits, E.; Baer, R.; Neuhauser, D. *Science* **2004**, *303*, 1849−1851. (d) Kottas, G. S.; Clarke, L. I.; Horinek, D.; Michl, J. *Chem. Rev.* **2005**, *105*, 1281−1376.
(4) Jiménez, M. C.; Dietrich-Buchecker, C.; Sauvage, J.-P. *Angew. Chem., Int. Ed.* **2000**, *39*, 3284−3287.
(5) Feringa, B. L., Ed. *Molecular Switches*; Wiley-VCH: Weinheim, 2001.
(6) Badjić, J. D.; Balzani, V.; Credi, A.; Silvi, S.; Stoddart, J. F. *Science* **2004**, *303*, 1845−1849.
(7) (a) Koumura, N.; Zijlstra, R. W. J.; van Delden, R. A.; Harada N.; Feringa, B. L. *Nature* **1999**, *401*, 152−155. (b) Koumura, N.; Geertsema, E. M.; Meetsma, A.; Feringa, B. L. *J. Am. Chem. Soc.* **2000**, *122*, 12005−12006. (c) van Delden, R. A.; ter Wiel, M. K. J.; Pollard, M. M.; Vicario, J.; Koumura, N.; Feringa, B. L. *Nature* **2005**, *437*, 1337−1340.
(8) Kelly, T. R.; De Silva, H.; Silva, R. A. *Nature* **1999**, *401*, 150−152.
(9) (a) Leigh, D. A.; Wong, J. K. Y.; Dehez, F.; Zerbetto, F. *Nature* **2003**, *424*, 174−179. (b) Hernández, J. V.; Kay, E. R.; Leigh, D. A. *Science* **2004**, *306*, 1532−1537.
(10) Fletcher, S. P.; Dumur, F.; Pollard, M. M.; Feringa, B. L. *Science* **2005**, *310*, 80−82.
(11) Thordarson, P.; Bijsterveld, E. J. A.; Rowan A. E.; Nolte, R. J. M. *Nature* **2003**, *424*, 915−918.
(12) (a) Ichimura, K.; Oh, S.-K.; Nakagawa, M. *Science* **2000**, *288*, 1624−1626. (b) Oh, S.-K.; Nakagawa, M.; Ichimura, K. J. *Mater. Chem.* **2002**, *12*, 2262−2269.
(13) Rosario, R.; Gust, D.; Garcia, A. A.; Hayes, M.; Taraci, J. L.; Clement, T.; Dailey, J. W.; Picraux, S. T. *J. Phys. Chem. B* **2004**, *108*, 12640−12642.

employed an azobenzene oligomer to deflect the tip of an atomic force microscope.[15] Azobenzene switches have been covalently incorporated into polymeric liquid crystal films to effect a phase transition leading to a photoinduced contraction of the film.[16] Recently, Ho, Stoddart, and co-workers effectively used surface-bound rotaxane-based molecular muscle mimics to generate a deflection in microscopic cantilever beams.[17] The use of a force for the transmission of a mechanical movement from a nanoscopic to a mesoscopic (or macroscopic) process looks conceptually easier for translational movement than for rotation. Nevertheless, we recently reported that the collective action of molecular motors embedded in a liquid crystal matrix can be harnessed to rotate microparticles which exceed the motor by 10 thousand times in size.[18]

Cholesteric (or chiral nematic) liquid crystals (LCs) are characterized by large, supramolecular, chiral organization, the chirality of which is indicated by the sign and magnitude of the cholesteric pitch. The pitch (p, the length of one turn of the cholesteric helix) is dependent on: (1) the concentration (c) of the dopant, (2) the helical twisting power (β) of the dopant, and (3) the enantiomeric excess (ee) of the dopant, following eq 1.

$$p = [\beta \cdot c \cdot (\text{ee})]^{-1} \quad (1)$$

An intrinsic property of any chiral dopant is the helical twisting power, which indicates how efficient this molecule is in inducing a chiral orientation in the LC material. Molecules which bear a structural resemblance to the mesogenic host often possess a significant helical twisting power.[19] Previously, overcrowded alkene-based molecular motors and switches have been shown to be efficient chiral bistable dopants for inducing helical (cholesteric) ordering in nematic liquid crystalline films.[20] Using switches with opposite helical twisting powers, photochemical switching between cholesteric phases with opposite chirality was readily achieved.[21] The use of the first generation of overcrowded alkene-based molecular motors as chiral dopants in nematic LC hosts allowed the creation of colored LC films, the color of which could be selectively adjusted with the motor molecule.[22] Recently, we reported a new class of second generation molecular motors, with the fluorene moiety as a common feature in the lower half of the molecule.[23] The fluorene moiety was chosen for the lower part, because it has a structural resemblance to the biphenyl core of commonly used mesogenic hosts, and therefore might enhance its interactions with the LC host. Indeed, our preliminary investigations into one motor in this series (compound **1**) validated this prediction by displaying very large helical twisting powers for both stable and unstable forms of the motor.[18]

Important features of motor **1** are a *P*-helical structure, a single stereogenic center in the upper part, a central carbon−carbon double bond that functions as the axis of rotation, and a symmetrical lower part.

In its stable form **1a**, the phenyl substituent adopts a pseudoaxial orientation to avoid steric repulsion with the fluorene lower half (Scheme 1). Upon irradiation with UV light

Scheme 1. Unidirectional Rotary Cycle of Fluorene-Based Motor **1**

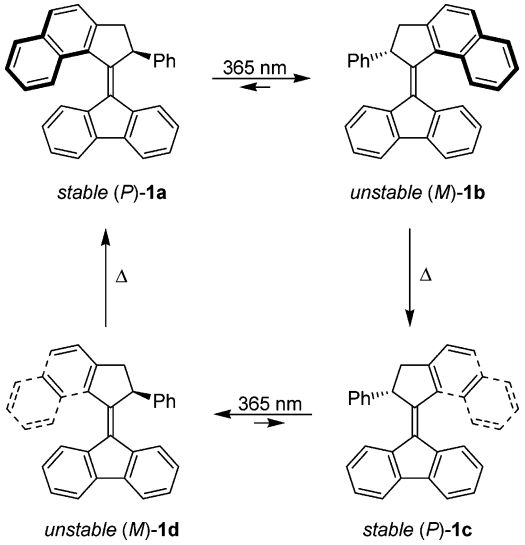

($\lambda = 365$ nm) a photochemical isomerization around the central double bond occurs to form **1b** with inversion of the molecule's helicity ($P \rightarrow M$). Simultaneously, the exocyclic phenyl substituent is forced to adopt a strained pseudoequatorial orientation, due to a change in conformation of the five-membered ring.[23] A subsequent thermal helix-inversion ($M \rightarrow P$), driven by release of this strain, occurs readily at room temperature ($t_{1/2} = 9.9$ min in toluene), leading to **1c**. Since **1a** and **1c** are degenerate forms, this sequence can be considered as the first 180° part of the rotary cycle. In this new class of motors (Figure 1), the speed of the rotation could be adjusted by changing the ring size or the substituent at the stereogenic center (phenyl in **1**) in the upper half of the molecule.

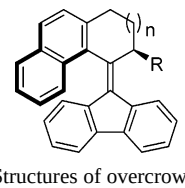

	R	n
(2'*S*)-(*P*)-**1**	Ph	0
(2'*R*)-(*P*)-**2**	Me	0
(2'*S*)-(*P*)-**3**	*i*-Pr	0
(2'*R*)-(*P*)-**4**	Me	1

Figure 1. Structures of overcrowded alkene-based molecular motors used as liquid crystal dopants.

(14) Berná, J.; Leigh, D. A.; Lubomska, M.; Mendoza, S. M.; Pérez, E.; Rudolf, P.; Teobaldi, G.; Zerbetto, F. *Nat. Mater.* **2005**, *4*, 704−710.
(15) Hugel, T.; Holland, N. B.; Cattani, A.; Moroder, L.; Seitz, M.; Gaub, H. E. *Science* **2002**, *296*, 1103−1106.
(16) (a) Yu, Y.; Nakano, M.; Ikeda, T. *Nature (London)* **2003**, *425*, 145. (b) Ikeda, T.; Nakano, M.; Yu, Y. L.; Tsutsumi, O.; Kanazawa, A. *Adv. Mater.* **2003**, *15*, 201−205. (c) Ikeda, T. *J. Mater. Chem.* **2003**, *13*, 2037−2057 and references therein. (d) Yu, Y.; Ikeda, T. *Angew. Chem., Int. Ed.* **2006**, *45*, 5416−5418 and references therein.
(17) (a) Huang, T. J.; Brough, B.; Ho, C.-M.; Liu, Y.; Flood, A. H.; Bonvallet, P.; Tseng, H.-R.; Baller, M.; Magonov, S.; Stoddart, J. F. *Appl. Phys. Lett.* **2004**, *85*, 5391−5393. (b) Liu, Y.; Flood, A. H.; Bonvallet, P. A.; Vignon, S. A.; Northrop, B. H.; Tseng, H.-R.; Jeppesen, J. O.; Huang, T. J.; Brough, B.; Baller, M.; Magonov, S.; Solares, S. D.; Goddard, W. A.; Ho, C.-M.; Stoddart, J. F. *J. Am. Chem. Soc.* **2005**, *127*, 9745−9759.
(18) Eelkema, R.; Pollard, M. M.; Vicario, J.; Katsonis, N.; Serrano Ramon, B.; Bastiaansen, C. W. M.; Broer, D. J.; Feringa, B. L. *Nature* **2006**, *440*, 163.
(19) (a) Solladié, G.; Zimmermann, R. G. *Angew. Chem., Int. Ed. Engl.* **1984**, *23*, 348−362. (b) Superchi, S.; Donnoli, M. I.; Proni, G.; Spada, G. P.; Rosini, C. *J. Org. Chem.* **1999**, *64*, 4762−4767 and references therein.
(20) Huck, N. P. M.; Jager, W. F.; de Lange, B.; Feringa, B. L. *Science* **1996**, *273*, 1686−1688.
(21) Feringa, B. L.; Huck, N. P. M.; van Doren, H. A. *J. Am. Chem. Soc.* **1995**, *117*, 9929−9930.
(22) van Delden, R. A.; Koumura, N.; Harada, N.; Feringa, B. L. *Proc. Natl. Acad. Sci. U.S.A.* **2002**, *99*, 4945−4949.
(23) (a) Vicario, J.; Meetsma, A.; Feringa, B. L. *Chem. Commun.* **2005**, 5910. (b) Vicario, J.; Walko, M.; Meetsma, A.; Feringa, B. L. *J. Am. Chem. Soc.* **2006**, *128*, 5127−5135.

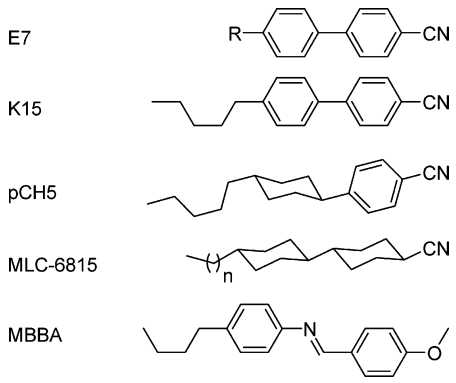

Figure 2. General structures of mesogenic hosts. E7 is a mixture of four compounds, with R = *n*-C_5H_{11}, *n*-C_7H_{15}, *n*-$C_8H_{17}O$, 4′-*n*-C_5H_{11}−C_6H_4.[26] The exact composition of the MLC-6815 mixture is unknown; bicyclohexylnitrile compounds are among its main constituents.

Table 1. Helical Twisting Powers of Fluorene-Based Dopants **1**−**4**

entry	dopant[a]	β_M (μm^{-1})[b]
1	(*P*)-**1**	+90
2	(*M*)-**2**	−56
3	(*P*)-**3**	+43
4	(*M*)-**4**	0

[a] Stable forms. [b] Measured in E7 at ambient temperature.[25]

In a preliminary investigation[18] we showed that when this rotary cycle was initiated while the motor was embedded in a liquid crystalline matrix, it generated an unprecedented rotational reorganization of the LC film. Strikingly, this remarkable rotational reorganization could be used to perform work by rotating particles on the film, thereby mediating work done at the molecular level to work at the macroscopic scale, using light as the fuel. Here, we wish to report our investigations on key structural features of motors capable of bringing forth this rotational movement, limitations of the system, and additional investigations on how the rotation of the LC texture influences the orientation of particles placed on its surface.

Results

Rotational Reorganization of Liquid Crystalline Films. The structures of optically active overcrowded alkene-based molecular motors are shown in Figure 1.[24] The helical twisting powers of overcrowded alkenes **1**−**4** were determined in E7 (Figure 2), as this LC host shows liquid crystallinity at room temperature and over a broad temperature range (Table 1).[25]

Most of these motors showed very high helical twisting powers, up to an order of magnitude higher than for previously reported overcrowded alkene-based switches.[21] The most effective cholesteric induction was found for methyl-substituted motor **2** ($\beta_M = 56\ \mu m^{-1}$, entry 2) and phenyl-substituted motor **1** ($\beta_M = 90\ \mu m^{-1}$, entry 1). Surprisingly, rather small changes in the structure can drastically affect the dopant behavior, as no cholesteric induction was found using six-membered upper half analogue **4** (entry 4). This indicates that the conformation of the upper part of the motor also drastically influences the cholesteric induction.

(24) For the synthesis, resolution, and characterization of motors **1**−**4**, see ref 23.
(25) Helical twisting powers were determined using the Grandjean−Cano method. See Dierking, I. *Textures of Liquid Crystals*; Wiley-VCH: Weinheim, 2003 and the Supporting Information for details.

Table 2. Helical Twisting Powers of Motor **1** in Various LC Hosts[a]

entry	LC host	β_M (μm^{-1})
1	E7	90
2	K15	137
3	pCH5	144
4	MLC-6815	75
5	MBBA	89

[a] The stable form of **1** was measured, at ambient temperature.

The helical twisting power of phenyl-substituted motor (2′*S*)-(*P*)-**1** was determined in a variety of liquid crystal hosts (Figure 2, Table 2). In all cases high helical twisting powers were obtained, with particularly high values in pentylbiphenylnitrile (K15) and its partially hydrogenated analogue pCH5 (entries 2 and 3). Even in MBBA, an LC host with a very different core structure, large cholesteric induction was observed (entry 5). However, due to an elongated conjugation in its core, MBBA is transparent only over 400 nm, which makes it useless as an LC host material for photochemical experiments with these photoactive guest compounds.

A second requirement for effective switching of liquid crystalline organization using a bistable chiral dopant is a large difference in helical twisting power between its isomeric forms. The helical twisting power of the unstable form of motor **1** was determined in E7, again using the Grandjean−Cano technique.[25] Due to a low free energy of activation of the thermal helix inversion step, it was impossible to isolate the unstable isomer in pure form and measure its helical twisting power. Consequently, the cholesteric induction by the photostationary state mixture after UV irradiation was studied. In isotropic solution, irradiation of the motor using UV light was found to lead to photostationary states with unstable-to-stable ratios of at most 86:14 ($\lambda = 365$ nm, toluene-d_8), depending on the solvent and the wavelength of irradiation.[23b] When (2′*S*)-(*P*)-**1** was irradiated while dissolved in the LC host, the composition of the photostationary state could not be determined because of the fast thermal helix inversion of the motor.[27] The apparent PSS of motor (2′*S*)-**1** was found to have a helical twisting power of over $-59\ \mu m^{-1}$ at room temperature (β_M, E7). Moreover, the sign of the cholesteric helicity was found to be opposite from that obtained using the stable isomer of the motor as a dopant.[28] To the best of our knowledge, this is the largest difference in helical twisting power ever observed between the two forms of a bistable dopant.[29,30] This also verifies that the induced cholesteric helicity is closely related to the helicity of the molecular motor,[31] as the molecular helicity also changes sign upon photochemical isomerization (Scheme 1, stable (*P*)-**1a** to unstable (*M*)-**1b**). When the LC films were allowed to stand at room temperature for over 45 min, the magnitude and sign of

(26) For the structure and composition of E7, see Lee, H.-K.; Kanazawa, A.; Shiono, T.; Ikeda, T. *Chem. Mater.* **1998**, *10*, 1402−1407.
(27) In similar overcrowded alkene-based chiral dopant systems, compared to the isotropic phase only slight changes in photostationary state composition were found when the irradiation was carried out in the LC phase. See: van Delden, R. A.; van Gelder, M. B.; Huck, N. P. M.; Feringa, B. L. *Adv. Funct. Mater.* **2003**, *13*, 319−324.
(28) The sign of the cholesteric phase was determined using a contact method; see Supporting Information for details.
(29) (a) Yokoyama, Y.; Sagisaka, T. *Chem. Lett.* **1997**, 687−688. (b) Sagisaka, T.; Yokoyama, Y. *Bull. Chem. Soc. Jpn.* **2000**, *73*, 191−196.
(30) Pieraccini, S.; Gottarelli, G.; Labruto, R.; Masiero, S.; Pandoli, O.; Spada, G. P. *Chem.—Eur. J.* **2004**, *10*, 5632−5639.
(31) Although a correlation between molecular and cholesteric helicity is frequently observed, exceptions have been reported. For a review on LC dopants, see: Eelkema, R.; Feringa, B. L. *Org. Biomol. Chem.* **2006**. Published online September 5, 2006; http://dx.doi.org/10.1039/b608749c.

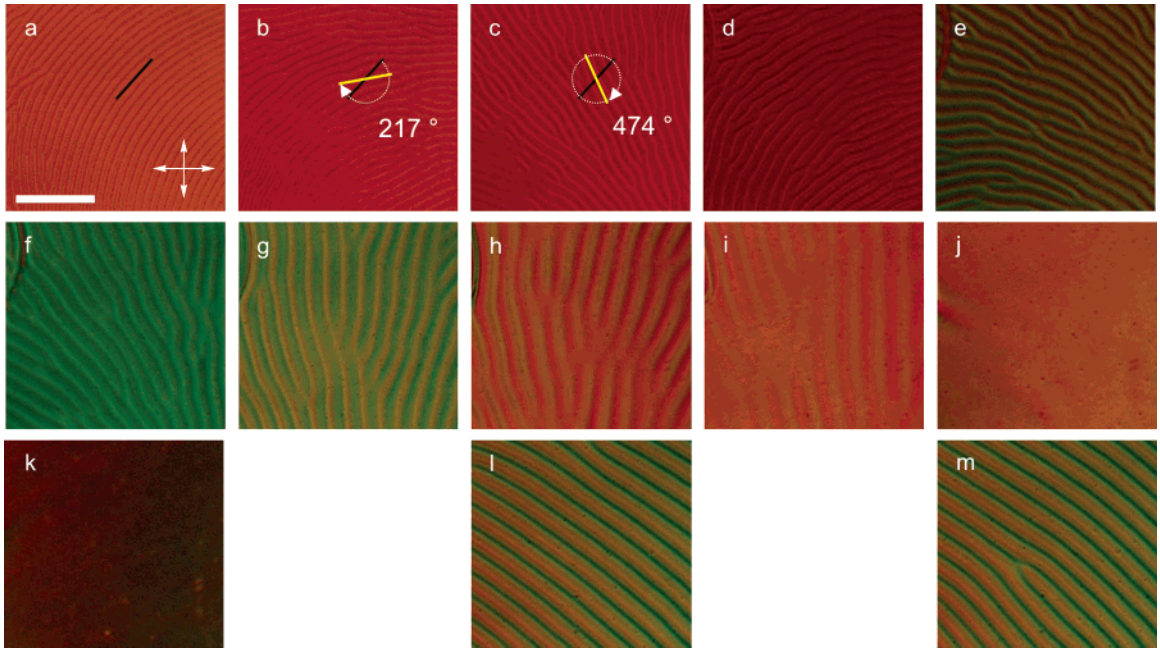

Figure 3. Rotational reorganization of a cholesteric texture. Shown here are optical micrographs of an aligned thin film of E7 doped with 1 wt % of (2′*S*)-(*P*)-**1a**. The pictures were taken at 15 s intervals during irradiation with 365-nm light and show a clockwise rotation. Black and yellow reference lines are used for initial and rotated texture orientation, respectively (pictures a, b, and c). After recording picture *k*, the sample was placed directly under the UV lamp for 10 min, resulting in texture l. Continuation of irradiation under the microscope for an additional 2 min resulted in no orientational change (picture m), suggesting that the photostationary state was reached. Scalebar, 50 μm. The crossed arrows indicate the directions of the crossed polarizers.

the cholesteric pitches returned to their original values without exception, resulting from the thermally induced helix inversion of the motor (Scheme 1), unstable (*M*)-**1b** to stable (*P*)-**1c**) used as a guest. This cycle was repeated over 10 times without deterioration of the measured β.

When a thin cholesteric LC film of E7 doped with 1 wt % **1** was placed on top of a glass slide covered with a unidirectionally rubbed polyimide alignment layer, a polygonal fingerprint texture was observed,[32] that is typical for alignment of the cholesteric helix axis parallel to the surface.[33]

During irradiation at $\lambda = 365$ nm under the microscope the polygonal texture reorganized in a rotational (clockwise) fashion in response to the isomerization of the motor and the subsequent modification of its helical twisting power (Figure 3). The lines of the polygonal texture (corresponding to a half pitch (*p*)) made several full turns, and eventually faded out. After prolonged irradiation for 10 min directly under the UV lamp to make use of light of a higher intensity, the rotating lines reappeared, and the helicity of the cholesteric liquid crystalline phase had inverted (Figure 3).[28]

During the initial phase of this reorganization, the distances between the lines in the texture also became larger. This can be expected from the formation of (*M*)-**1b** which, because of its lower β-value, would induce a lengthening of the helical pitch. As a result, during the photochemical conversion of **1a** ($\beta_M = +90\ \mu m^{-1}$) to **1b** ($\beta_M > -59\ \mu m^{-1}$), a mixture with an effective $\beta_M = 0\ \mu m^{-1}$ and consequently $p = \infty$ is formed at a certain stage, which explains the disappearance of the cholesteric texture. When the lines reappeared after fading out, the distances between the lines decreased until the lines stopped rotating, which is likely to be caused by reaching a photostationary state of the motor. When the irradiation was ceased, the cholesteric textures started to rotate in the opposite direction (counterclockwise) (Figure 4). During this process, the lines faded out and reappeared again. They stopped rotating after 45 min, showing that this reverse process takes place in response to the thermal helix inversion of **1b**, leading to the formation of **1c**. This sequence was repeated over 40 times with different samples. The textures always rotated clockwise during irradiation and counterclockwise during the thermal isomerization step. Exchanging (2′*S*)-(*P*)-**1a** for its enantiomer (2′*R*)-(*M*)-**1a** induced rotations in the opposite directions, unambiguously demonstrating that the direction of rotation of the LC texture is determined by the direction of change in helical twisting power of the motor.

To assess the generality of this phenomenon chiral overcrowded alkenes **2**−**4** were tested for their ability to induce these effects. Molecular motors **2** and **3** were found to induce rotational reorganizations of the liquid crystalline phase, similar to those observed for motor **1**. (*M*)-**2** induced a counterclockwise rotation during the photochemical step, whereas its enantiomer (*P*)-**2** induced the clockwise reorganization, as did (*P*)-**3** (Table 3). Alternatively, motor **4** generated no polygonal texture when mixed with E7 and examined through a polarizing microscope. Instead a nematic texture was observed that did not change appearance upon irradiation with 365-nm light. This is consistent with the observation that neither **4** nor its PSS_{365} has a measurable helical twisting power.

To explore whether these rotational effects extend beyond the use of overcrowded alkene-based unidirectional rotary molecular motors as chiral dopants, a known chiral switch with

(32) The liquid crystal mixture is applied as a thin film on the substrate which is coated with buffed polyimide. The opposite side of the liquid crystal is against air. The combination of both interfaces induces the chiral nematic liquid crystal to align in a so-called fingerprint texture with the helix axes parallel to the substrate surface in a basically monolithic orientation with a few domain walls at surface defects. The anchoring of the LC to the unidirectionally rubbed polyimide alignment layer thus provides a preferred orientation of the helix axes perpendicular to the rubbing direction.

(33) Dierking, I. *Textures of Liquid Crystals*; Wiley-VCH: Weinheim, 2003.

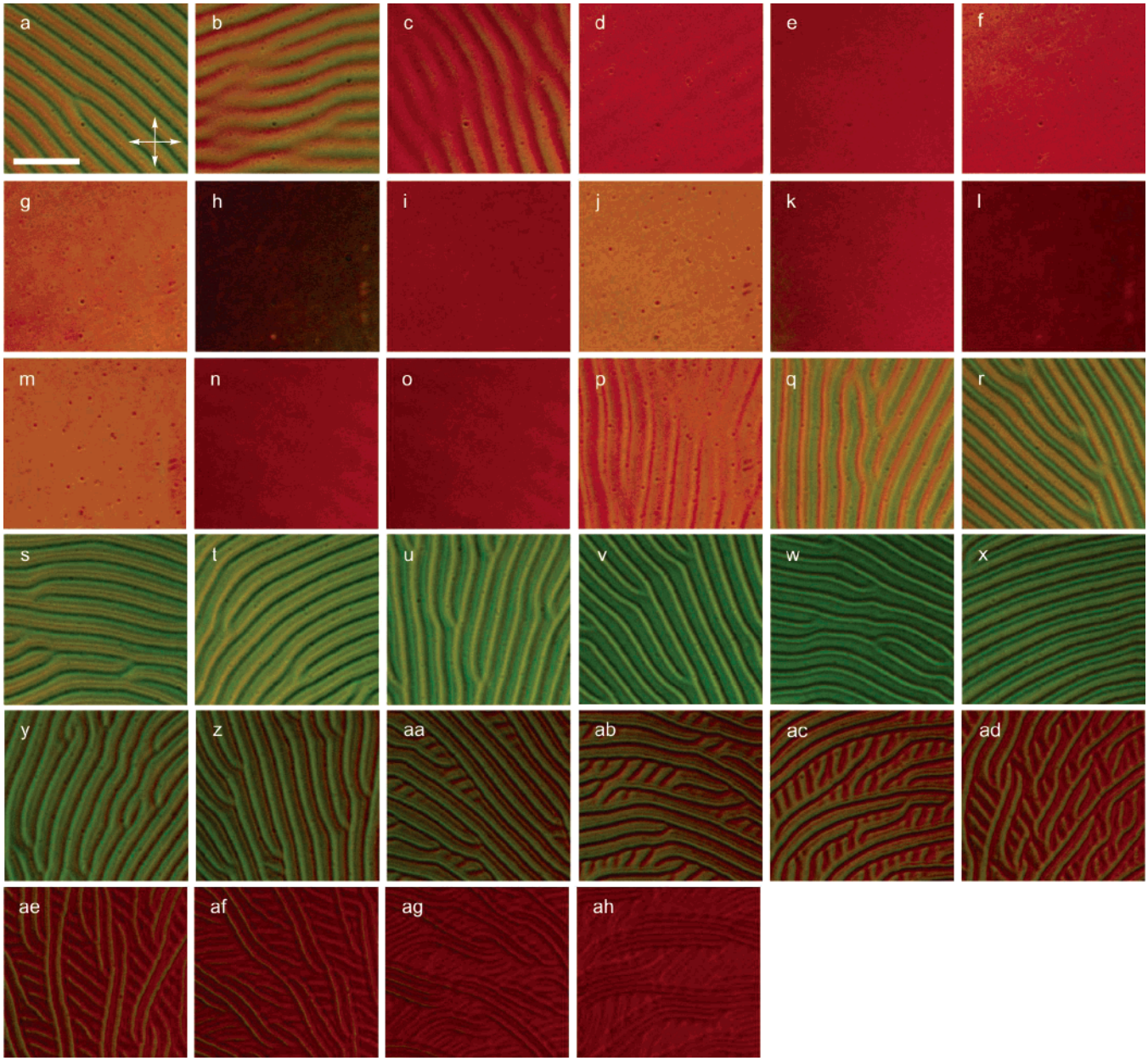

Figure 4. Rotational reorganization of a cholesteric texture following thermal isomerization of the molecular motor (**1b** → **1c**). Shown here is the same sample as in Figures 3, after stopping irradiation. The pictures were taken at 15 s intervals and show a counterclockwise rotation. Scalebar, 50 μm. The crossed arrows indicate the directions of the crossed polarizers.

Table 3. Rotational Reorganization Resulting from the Photochemical Isomerization of the Chiral Dopant[a]

entry	dopant	absolute configuration[b]	β_M (μm^{-1})[b]	$\Delta\beta$	rotation[c]
1	**1**	*P*	+90	<0	↷
2	**1**	*M*	−90	>0	↶
3	**2**	*M*	−56	>0	↶
4	**2**	*P*	+56	<0	↷
5	**3**	*P*	+43	<0	↷
6	**5**	*S*	−25	>0	↶

[a] Setup: λ = 365 nm irradiation, E7 LC host, 0.5−2 wt % chiral dopant. [b] Of the initial state of the dopant. [c] Direction of rotation: ↷ = clockwise, ↶ = counterclockwise.

Scheme 2

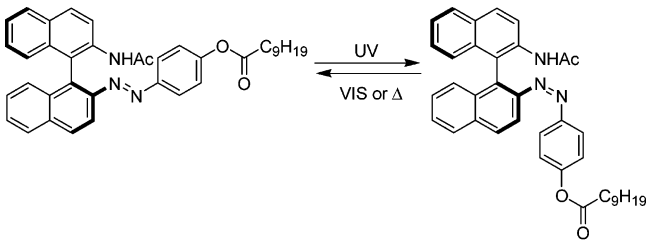

(*S*)-*E*-**5** (*S*)-*Z*-**5**

a completely different structure was synthesized[34] and tested. Chiroptic switch (*S*)-**5** possesses axial chirality through its binaphthyl moiety and an azobenzene switching unit that can undergo an E to Z isomerization under the influence of UV light (Scheme 2). The reverse Z to E isomerization can be effected using longer wavelength light or heat. This switch was first reported by Gottarelli and Spada to be an effective chiral dopant, especially in bicyclohexylnitrile LC hosts, where it

(34) See the Supporting Information for details.

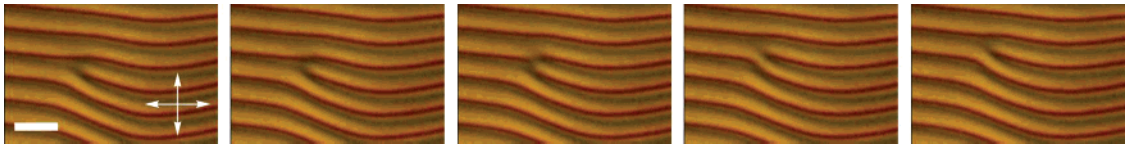

Figure 5. Single defect moving through a polygonal texture. The film consists of E7 doped with (*S*)-**5**, during the Z to E isomerization step. The images were recorded at 0.75 s intervals; scalebar, 50 μm. The crossed arrows indicate the directions of the crossed polarizers.

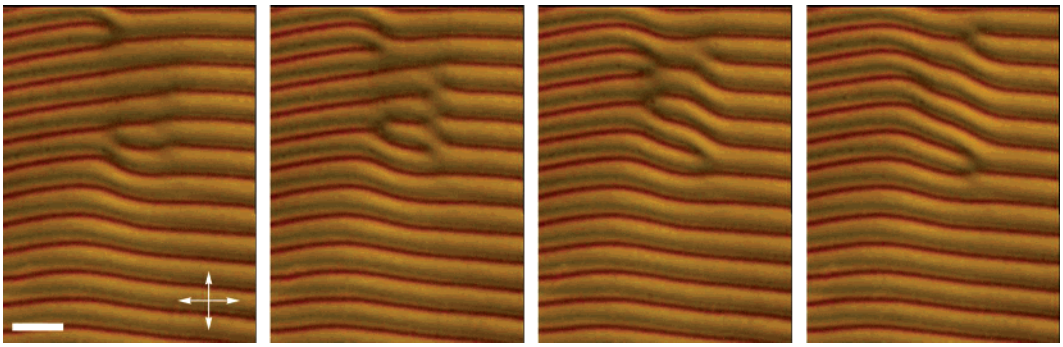

Figure 6. Multiple defects moving through the same film as that in Figure 5. The images were recorded at 1.0 s intervals; scalebar, 50 μm. The crossed arrows indicate the directions of the crossed polarizers.

induced an inversion of helical screw sense upon E to Z isomerization.[30]

For direct comparison with the results of our previous investigations, the cholesteric induction of (*S*)-E-**5** in bi- and terphenylnitrile LC host E7 was measured, revealing it to be less effective than in the reported bicyclohexylnitrile mesogenic host.[30] The (*S*)-E form of **5** has a helical twisting power (β_M, E7) of -25 μm^{-1}, which changed to -11 μm^{-1} in the photostationary state upon irradiation with 365-nm UV light when (partial) photoisomerization to (*S*)-Z-**5** occurs. Irradiation with longer wavelength light ($\lambda = 430$ nm) reversed this process and led to a photostationary state with an excess of the E isomer and an apparent helical twisting power of -22 μm^{-1}. Heating the sample resulted in a full recovery of the initial pitch, indicating a complete conversion to the more stable E form. In contrast to its reported behavior in the bicyclohexylnitrile LC host, this dopant did not induce an inversion of cholesteric screw sense in E7. Applying a 1 wt % mixture of the E form of this switch with E7 to a unidirectionally rubbed polyimide-coated glass plate led to the formation of polygonal textures similar to those observed for the overcrowded alkene-based molecular motors. Due to the lower helical twisting power of this dopant the texture bands are broader. Irradiation with UV light ($\lambda =$ 365 nm) resulted in a counterclockwise rotational reorganization of the polygonal texture with concomitant widening of the textural features. Subsequent heating or irradiation with 430-nm light led to the narrowing of the polygonal texture, with a concomitant clockwise rotational process. These observations confirm that the rotational reorganization is directly linked to the reversible change in helical twisting power of the chiral dopant. The results of the irradiation experiments of these switches and motors are summarized in Table 3. Overall, a trend emerges in the relation between the direction of the change in helical twisting power and the direction of rotational reorganization of the polygonal texture. Negative changes in β (i.e. $\Delta\beta < 0$) result in clockwise rotational reorganizations, whereas positive changes in β (i.e. $\Delta\beta > 0$) result in counterclockwise rotation. This relation also holds for the thermally induced processes. For example, the thermal helix inversion step of (*M*)-**1b** has a positive β change ($-59 \rightarrow +90$ μm^{-1}), inducing a counterclockwise rotational reorganization of the LC film.

The cholesteric induction by the stable form of motor **1** is very large in a range of calamitic liquid crystalline hosts, as was previously described (Table 2). These LC materials were also tested for their rotational reorganization behavior. Motor (2′*S*)-(*P*)-**1** induced clockwise reorganizations during the irradiation with UV light ($\lambda = 365$ nm) and counterclockwise rotations during the thermally driven reverse reaction in all tested biphenylnitrile-based hosts (E7, K15, pCH5, MLC-6815, see Figure 2). In imine-based MBBA these processes hardly seemed to occur, probably because no significant amounts of the unstable form were generated due to the host's extended absorption in the visible region.

Cholesteric Mesophase Structural Defects and Possible Mechanism of Rotational Reorganization. Examination of the processes taking place in the LC film during the rotational reorganizations revealed a remarkable behavior of the defects present in the film. Figure 5 shows a series of optical micrographs of an LC film doped with (*S*)-5, during the Z to E isomerization process.

The defect is a disclination pair[35] moving through the film during the rotational process, jumping from one line to the next (Figure 5). The lines hardly rotate by themselves but rather move and change orientation drastically in response to the passing of a defect. In addition to singular defects there are also series of defects moving through the film, as shown in Figure 6. These effects were observed during all rotational reorganizations induced by both photochemically and thermally driven isomerizations of the motors.

On the basis of these observations a hypothesis for the mechanism of rotational reorganization of cholesteric LC films was formulated. In these systems, the pitch of the cholesteric helix has to increase[36] in response to the topology change and the concomitant change in β_M of the chiral dopant present in the LC matrix. A pitch change requires a rotational repositioning

(35) The defects resemble $\tau^{-1/2}\lambda^{+1/2}$ disclination pairs, see: Smalyukh, I. I.; Lavrentovich, O. D. *Phys. Rev. E* **2002**, *66*, 051703.
(36) Or cholesteric helix has to decrease, depending on the stage of the process.

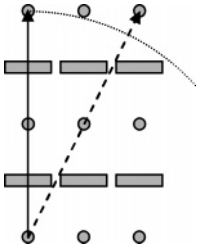

Figure 7. Change in direction of the cholesteric helix axis can result in a longer pitch. The solid arrow indicates the initial helix axis, the broken arrow, the new direction. Bars and dots represent local director orientations in the LC phase, with bars representing orientations parallel to the plane and dots perpendicular. The direction of rotation shown in the model was arbitrarily chosen.

of the mesogens perpendicular to the helix axis that is cumulative along this axis. This means that, going further along this axis, one mesogen has to reorient even more than the one before. Therefore, even a slight change in helical pitch would result in an enormous reorganization of all mesogens throughout the matrix, which is likely to be unfavorable. However, if the helix axis would change direction, it could attain a longer pitch while minimizing the orientational reorganization of the mesogens, as the hypotenuse of a right-angled triangle is longer than either of its legs (Figure 7).[37] The molecules oriented perpendicular to the air and substrate interface do not undergo any reorientation at all.

Although changing the helix axis direction results in a longer pitch, it also changes the angle of some of the local directors with respect to the cholesteric helix axis (Figures 7 and 8). The local directors perpendicular to the plane are already in the favorable 90° angle with respect to the cholesteric helix axis, but the local directors parallel to the plane obtain an unfavorable deviation from this desired 90° angle resulting from the orientation change of the cholesteric helix (Figure 8a, broken arrow). In response to this displacement from equilibrium, the local director angle has to change (Figure 8b) and a local reorganization has to take place to align the regions with similar directors (Figure 8c−f). The latter process can be considered as a defect propagating through the superstructure. Overall, this results in a pitch lengthening accompanied by a change in orientation of the cholesteric helix axis.

Rotation of Microscale Particles. Microparticles with a typical size ranging from 10 to 60 μm were placed on top of a liquid crystalline film doped with either motor (*P*)-**1** or motor (*M*)-**2**, and their behavior was monitored during the reorganization steps. In particular, glass rods of three different sizes (diameters 3.2, 5.0, and 10.0 μm) were placed on these doped liquid crystal films. Upon irradiation, the two smaller types rotated in the same direction as the rotating cholesteric textures. Figure 9 shows the typical rotary motion for one of these rods.

When the irradiation was stopped, the particles started to rotate in a counterclockwise fashion, again following the direction of rotation of the cholesteric texture on which they were placed (Figure 10).

Only the rods with 10 μm diameter did not rotate on the film during either irradiation or thermal steps of the process. Rotation of other micrometer-sized particles of different shape and composition was also observed, including glycine, ground NaCl, and Na_2SO_4 crystals. On irradiated films with rotating particles, there were always a number of particles that did not move. In some cases this seemed to be the result of sinking of the particles in the LC film. However, there were also particles of sizes similar to that of their rotating counterparts that remained stagnant, indicating that not only the mass but possibly also the exact shape of the particles is crucial for their rotation.

Surface Structure of the Cholesteric Film. To investigate the mechanism by which light energy harvested on the molecular scale results in microscopic mechanical motion, the surface properties of the LC film were studied, as this is the interface through which the rotational motion is transmitted to the particles. An aligned cholesteric film consisting of E7 doped with motor (*P*)-**1** was examined by atomic force microscopy (AFM), which revealed a regular surface relief (Figure 11).

All studied cholesteric films were found to have a surface relief with a height of up to 20 nm and a typical periodicity of 5.5 μm. The same periodicity was also observed in the polygonal line textures found with optical microscopy, proving that this surface relief is associated with the cholesteric helix superstructure. There have been previous reports of surface corrugation of liquid crystalline films at the LC−air interface. However, they dealt with achiral smectic or glassy cholesteric films.[38,39] In the latter case microtomed samples were used, where the corrugation is likely to be the result of a preferred fracture path. The structures observed on the surfaces of smectic films are often the result of different physical phenomena, such as the appearance of defects to release stresses arising from variation

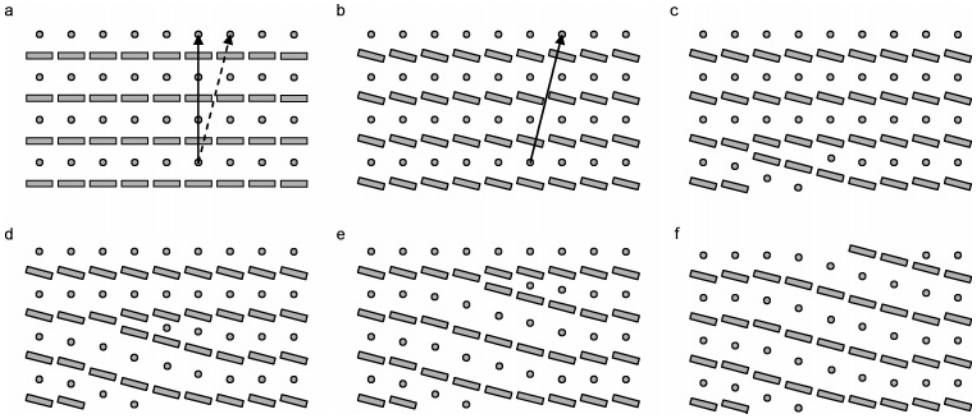

Figure 8. Proposed mechanism for rotational reorganization of cholesteric LC films. Bars and dots represent local director orientations. A change in helix axis direction results in a larger pitch (a and b), but also in unfavorable configurations of some of the local directors. To compensate for this, a defect (c) moves through the assembly, aligning the local areas with similar directors (c−f). Repetition of this process can result in continual rotation.

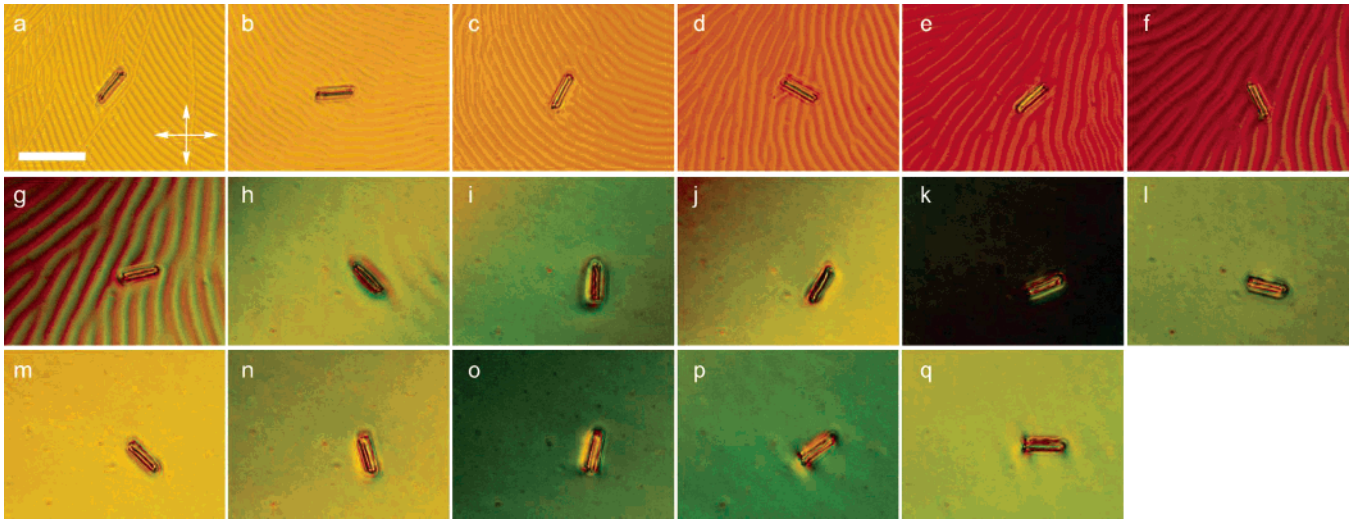

Figure 9. Optical micrographs of a glass rod rotating on an LC film doped with molecular motor **1**, during irradiation with UV light (λ = 365 nm). The rod and the cholesteric texture rotate in a clockwise fashion; the pictures were taken at 15 s intervals, except for frame q, which was recorded 11 s after p. During the depicted process, the rod made approximately 2.5 full turns. The dimensions of the rod are 5.0 × 28.4 μm; scalebar, 50 μm. Glass rod, 28 μm long, 5 μm in diameter. The crossed arrows indicate the directions of the crossed polarizers.

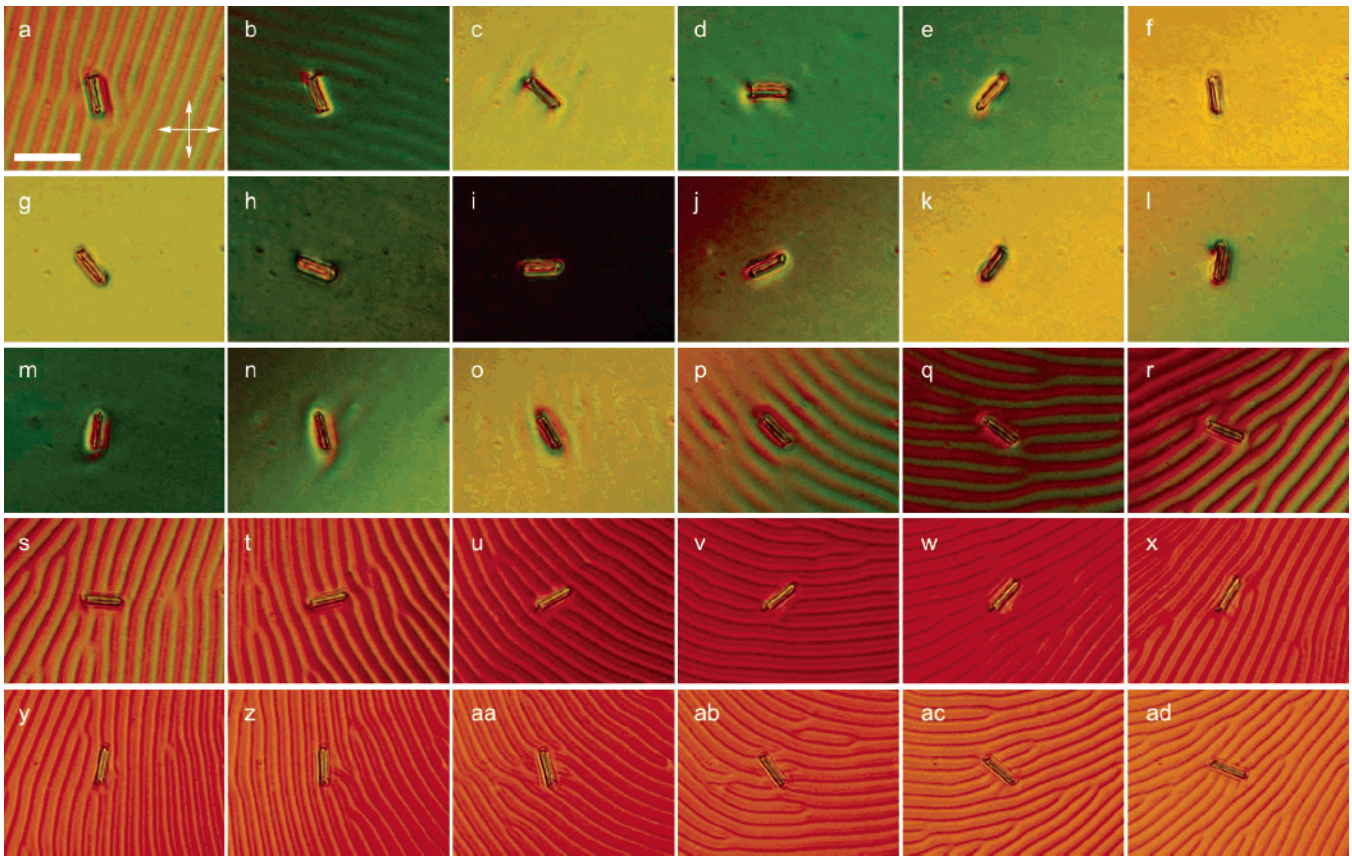

Figure 10. Optical micrographs of a glass rod rotating on an LC film doped with molecular motor **1**, during the thermal helix inversion of the motor. The rod and texture are the same as depicted in Figure 9, and were recorded after additional direct close-range irradiation (3 cm distance) with UV light (λ = 365 nm). The rod and the cholesteric texture rotate in a counterclockwise fashion; the pictures were taken at 15 s intervals. During the depicted process, the rod made approximately 1.8 full turns. Scalebar, 50 μm. Glass rod, 28 μm long, 5 μm in diameter. The crossed arrows indicate the directions of the crossed polarizers.

of anchoring geometries of the mesogens between the polymer-coated alignment surface and the LC−air interface.[38]

Rationale for the Formation of a Corrugated LC Surface. The presence of a chiral dopant in the liquid crystalline film results in a highly corrugated surface, with dimensions a few orders of magnitude larger than the typical size of its building blocks. In the absence of constraints, surface tension would flatten the film in order to minimize the surface area. As the surface modulation follows the pitch of the cholesteric helix, the constraints set by the orientation of the mesogens in this helix superstructure are most likely the cause of the formation of the high corrugations observed at the air−liquid interface.

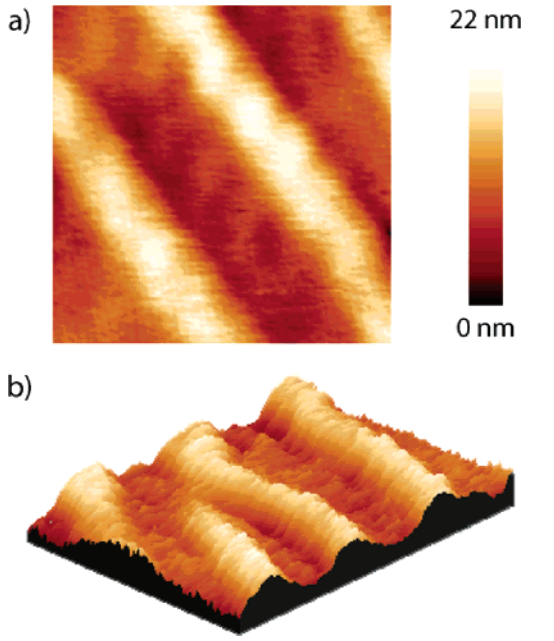

Figure 11. Surface structure of E7 doped with **1**, measured by AFM in noncontact mode. The height scalebar corresponds to both images. (a) The size of the image is 11 μm × 11 μm. (b) The size of the image is 14.7 μm × 11.1 μm. It shows a disclination pair defect. In both images, the relief correlated to the helical pitch has a height of 16 nm and a period of 5.0 μm. An additional periodic relief having a smaller height of about 3 nm and forming an angle of about 80° with the main relief is also distinguishable. This substructure could be created by periodic defects arising from antagonistic anchoring geometries between the polymer−LC interface and the LC−air interface. Such periodic defects have been previously described in smectic thin films.[34e]

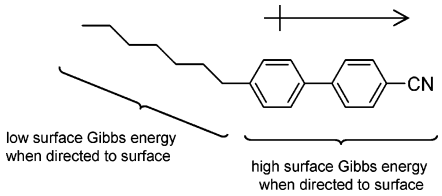

Figure 12. Polarization and contributions to surface Gibbs energy of cyanobiphenyl-based mesogens.

Cyanobiphenyl mesogens are polarized parallel to their molecular long axis, resulting in differences in surface energy between the cyanobiphenyl and alkyl parts of the molecules (Figure 12). In a cholesteric LC phase with the helix axis aligned parallel to the surface, there will be a distinct difference in surface energy of the liquid crystal, depending on the orientation of the LC molecules with respect to the LC−air interface (Figure 13a and b). The molecules aligned with their long axes perpendicular to the surface lower the local surface Gibbs energy by orienting themselves with the alkyl moiety toward the air. Competition between the local modulation of surface tension along the helix axis and the energetic cost of the curvature of the surface gives

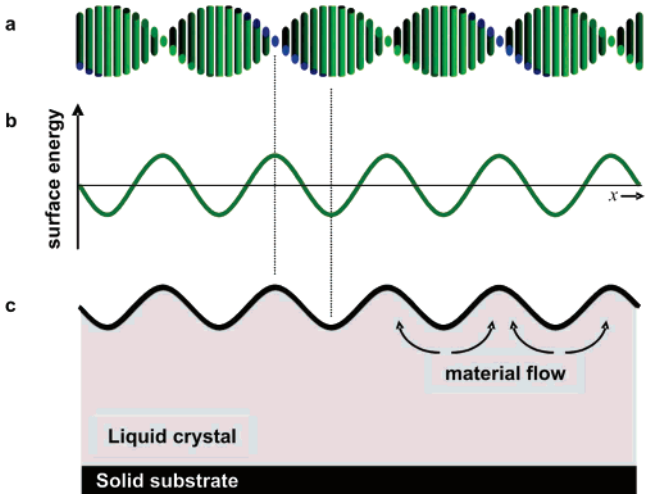

Figure 13. Schematics of the formation of a corrugated surface. (a) Average orientation of the LC molecules along the helical axis. (b) Periodic changes in the orientation of LC molecules at the surface result in a periodic surface energy profile. Due to the lower polarity of the alkyl moieties, molecules with an orientation perpendicular to the air−LC interface are most likely to lower the local surface energy. x corresponds to the helical axis. (c) A periodic surface energy gradient is at the origin of the curvature of the surface.

rise to a periodic relief modulation (Figure 13c), a physical phenomenon also at the origin of the well-known Marangoni effect.[40] As the helix periodicity and orientation change in response to photochemically or thermally induced topology changes of the molecular motor used as the chiral dopant, the areas of high and low surface tension will change accordingly, resulting in a modification of the surface pattern.

In an attempt to rationalize and thus eventually control the angular speed of a microsized particle placed on top of the doped LC, the angular reorganization of an arbitrarily chosen section of polygonal texture was determined over time,[41] both during irradiation (Figure 14a) and thermal steps (Figure 14b).

The variation of rotational speed of the LC texture over time can be rationalized with first-order kinetic laws since the rotational reorganization is caused by the (first order) photochemical and thermal conversions between the different forms of the motor. Combining this with eq 1, and the observation that the stable and unstable isomers of motor **1** (designated **1a** and **1b** in Scheme 1, respectively) have different helical twisting powers, leads to eq 2.[34] This equation describes the proportionality (γ) of the rotational displacement of the LC (θ_t) as a function of the helical twisting powers and concentrations of both isomers of the motor dopant, the rate constant of the reaction (k), and time (t). A numerical expression for the speed of rotation (ω_t) can be obtained by derivation of eq 2 (eq 3).

$$\theta_t \propto \gamma \cdot p_t^{-1} = \gamma \cdot (\beta_A [A]_t + \beta_B ([A]_0 - [A]_0 e^{-kt})) \quad (2)$$

$$\frac{d\theta}{dt} = \omega_t = \gamma \cdot \Delta\beta \cdot [A]_0 e^{-kt} \quad (3)$$

(37) As described above, we have observed a direct relation between changes in molecular helicity, changes in helicity of the cholesteric phase, and the direction of rotational reorganization. While with the model described in Figures 7 and 8 we can account for rotation of the texture, we cannot at this stage account for the direction of rotation.

(38) For AFM of smectic films, see: (a) Terris, B. D.; Twieg, R. J.; Nyuyen, C.; Sigaud, G.; Nguyen, H. T. *Europhys. Lett.* **1992**, *19*, 85−90. (b) Michel, J.-P.; Lacaze, E.; Alba, M.; de Boissieu, M.; Gailhanou, M.; Goldmann, M. *Phys. Rev. E* **2004**, *70*, 11709. (c) Choi, M. C.; Pfohl, T.; Wen, Z.; Li, Y.; Kim, M. W.; Israelachvili, J. N.; Safinya, C. R. *Proc. Natl. Acad. Sci. U.S.A.* **2004**, *101*, 17340−17344. (d) Designolle, V.; Herminghaus, S.; Pfohl, T.; Bahr, C. *Langmuir* **2006**, 22, 363−368.

(39) For AFM of glassy cholesteric films, see: (a) Bunning, T. J.; Vezie, D. L.; Lloyd, P. F.; Haaland, P. D.; Thomas, E. L.; Adams, W. W. *Liq. Cryst.* **1994**, *16*, 769−791. (b) Meister, R.; Hallé, M.-A.; Dumoulin, H.; Pieranski, P. *Phys. Rev. E* **1996**, *54*, 3771. (c) Boudet, A.; Mitov, M.; Bourgerette, C.; Ondarçuhu, T.; Coratger, R. *Ultramicroscopy* **2001**, *88*, 219−229.

(40) Guyon, E.; Hulin, J. P.; Petit, L.; Mitescu, C. D. *Physical Hydrodynamics*; Oxford University Press: Oxford, 2001.

(41) Automated data treatment is described in the Supporting Information.

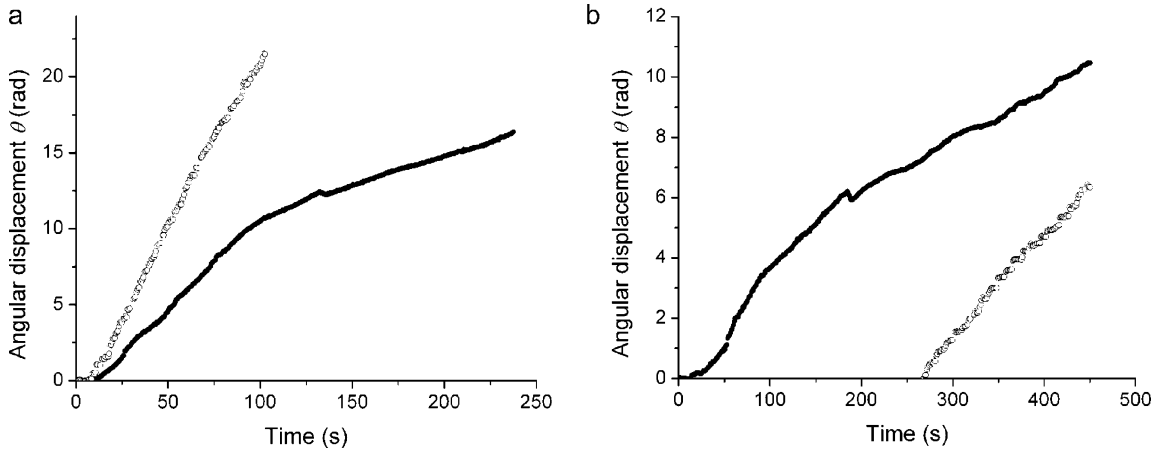

Figure 14. Angular displacement vs time of the texture of an LC film doped with molecular motor 1 (open dots) and a rod rotating on top of it (filled dots). (a) Shows the rotation during irradiation (365 nm); (b) shows the rotation of the same film and rod during the thermal step. All graphs show absolute angular displacement.

This shows that both speed and angular rotation of the texture depend on the difference in helical twisting power between the two interconverting forms, their initial concentrations, and the reaction rate constant. It also predicts an exponential dependence of the rotational displacement of the LC with respect to time. This was confirmed by successful fits of the experimental curves in Figure 14 with eq 2, using characteristic values for the system in terms of helical twisting powers and concentrations.

The angular displacement vs time of a particle rotating on top of the LC phase is also depicted in Figure 14. During the photochemical step, the rod made approximately 2.5 full rotations over the course of 4 min, which provides an average speed of 0.07 rad/s (Figure 14a). The thermal step was much slower at an average speed of 0.02 rad/s (Figure 14b). In both steps of this process, the rotational reorganization of the polygonal texture was faster than the rotary movement of the particle floating on top of it. After an initial period of acceleration in the photochemical step, an approximate 2:1 ratio in texture and rod displacements could be observed in both irradiation and thermal steps.[42] However, it is possible that on a longer time scale these speeds would equalize.[34] Both angular displacement vs time curves of the particle can thus be fitted by an exponential function, consistent with the exponential dependence of the LC speed over time. The constant ratio between the rotational speed of the rod and the LC film is indicative of the presence of nonlinearities in the friction process, which cannot be entirely described by fluid or viscous friction terms.[40] As such, there is a conceptual similarity between this system and the so-called "asynchronous rotational machine", where a stator drives the rotation of a rotor using a rotating magnetic field, and both the rotor and the magnetic field rotate at different but proportional speeds.[43]

Small deviations from these laws (eq 2 and 3) were observed in the rotational behavior of the rod; however, no further investigations concerning these phenomena had been conducted so far. One particularly pronounced irregularity in the rotational behavior of the rod is revealed after 130 s (Figure 14a). At this point the wormlike textures had already disappeared, and the rod momentarily stopped rotating, moved back slightly, and then resumed rotation in the original direction. Judging from the optical micrographs of this process, this behavior results from a change in interaction between the rod and the LC film (Figure 15a), which could be caused by a modification of surface tension. This phenomenon was observed in several cases, including the rotation of other glass rods and NaCl particles during both photochemical and thermal isomerization-induced reorganizations (Figures 14b and 15b).

Conclusions

The results presented in this article show that photochemically or thermally induced topology changes in a chiral dopant can induce a rotational reorganization of a cholesteric liquid crystalline film. This rotational movement can be applied to rotate objects 4 orders of magnitude larger than the chiral dopant, which clearly demonstrates that molecular motors and switches can perform rotational work.

The rotational reorganizations take place in response to the change of state of the dopant, with the direction of rotation depending on the sign of the dopant's change in helical twisting power. As such, in this system both the azobenzene switch and the rotary motors act as switches on the molecular scale. However, through its collective effect, the bistable dopants in the liquid crystalline matrix act as a motor, as they can generate a torque (and hence directed, controllable motion) on the embedded microscopic particles. Fluorene-based second-generation molecular motors are highly efficient bistable dopants for calamitic liquid crystals, showing enormous helical twisting powers depending on the structure of both dopant and mesogenic host. Helical twisting powers up to 144 μm^{-1} where obtained for the stable form of phenyl-substituted motor **1**, whereas the unstable form of **1** also displays a large helical twisting power. Moreover, the helical twisting powers of stable and unstable forms have opposite signs, allowing efficient switching between supramolecular helicities. Through analysis of the rotational behavior of rods and textures, a description of this behavior in terms of change in helical twisting powers and concentrations of both motor isomers and the rate constants of their interconversions was obtained, which might allow further control of this rotational behavior through rational design and might guide future applications of molecular motors.

(42) On the basis of this initial acceleration, the work done when the rod makes one full rotation during the photochemical step of the process was determined at 3.93×10^{-24} J. See Supporting Information for details.
(43) Basu, D. K., Ed. *Dictionary of Pure and Applied Physics*; CRC Press: Boca Raton, FL, 2000.

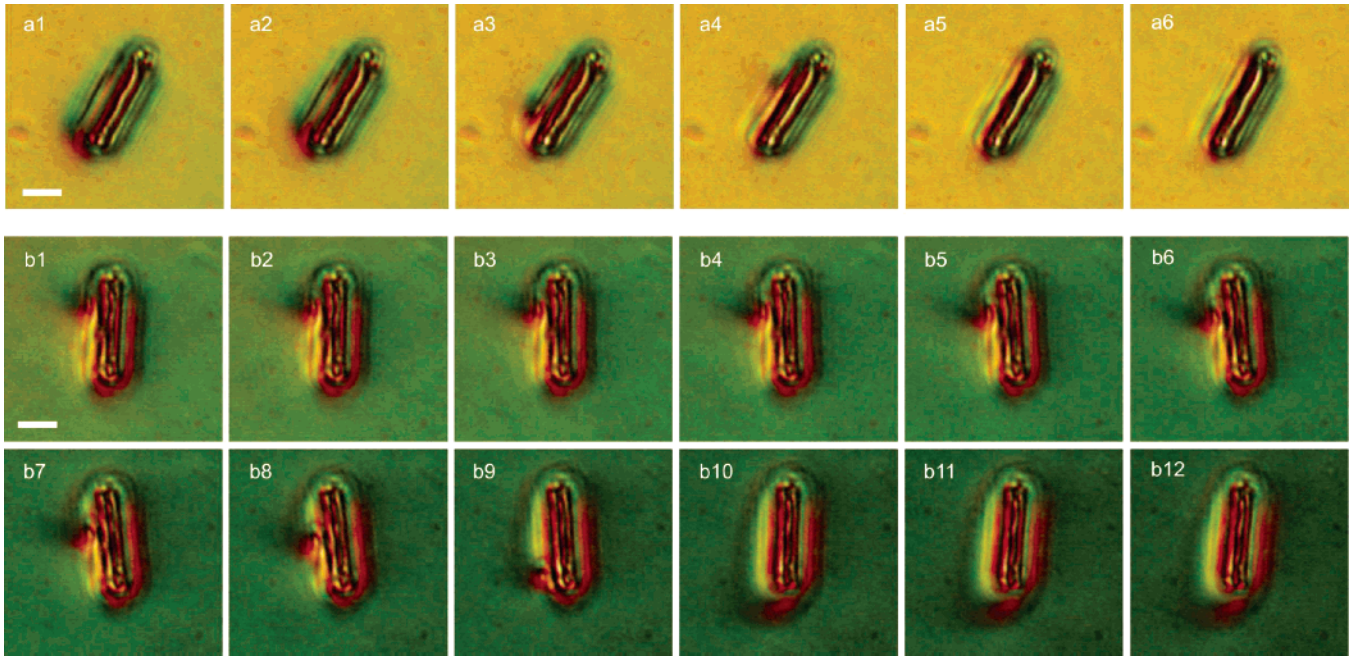

Figure 15. Change in interaction between the rod and the LC film (E7 doped with (2′*S*)-**1**). The pictures shown here were recorded during the processes depicted in Figures 9 and 10, at 0.5 s intervals. During both the irradiation step (a) and the thermal step (b) a change in the texture surrounding the rod is visible. In (a) the change is visible in a3−a5, in (b) in b6−b11; scalebar 10 μm; glass rod: 28 μm long, 5 μm in diameter.

Acknowledgment. This work was supported by grants from The Netherlands Organization for Scientific Research (NWO-CW) (R.E., B.L.F.), the Materials Science Centre (MSC^+) (M.M.P.), the Koerber Foundation (N.K., B.L.F.), the Departamento de Educación, Universidades e Investigación del Gobierno Vasco (J.V.), and the Dutch Polymer Institute (D.J.B.). LC material MLC-6815 was received as a gift from Merck, Darmstadt, for which they are gratefully acknowledged.

Supporting Information Available: Synthesis of **5**, experimental details for the preparation of LC films, determination of cholesteric pitch, analysis of particle rotation, AFM, automated picture processing, and determination of work performed. This material is available free of charge via the Internet at http://pubs.acs.org.

JA065334O